THE JOURNAL OF BIOLOGICAL CHEMISTRY
Vol. 276, No. 44, Issue of November 2, pp. 41310–41317, 2001
Printed in U.S.A.


# $\beta_1$-Adrenergic Receptor Association with the Synaptic Scaffolding Protein Membrane-associated Guanylate Kinase Inverted-2 (MAGI-2)

## DIFFERENTIAL REGULATION OF RECEPTOR INTERNALIZATION BY MAGI-2 AND PSD-95*

Received for publication, August 5, 2001
Published, JBC Papers in Press, August 28, 2001, DOI 10.1074/jbc.M107480200

**Jianguo Xu, Maryse Paquet, Anthony G. Lau, Jonathan D. Wood‡§, Christopher A. Ross‡, and Randy A. Hall¶**

*From the Department of Pharmacology, Rollins Research Center, Emory University School of Medicine, Atlanta, Georgia 30322 and the ‡Department of Psychiatry and Behavioral Sciences, Division of Neurobiology, The Johns Hopkins University School of Medicine, Baltimore, Maryland 21205*

**The $\beta_1$-adrenergic receptor ($\beta_1$AR) is known to be localized to synapses and to modulate synaptic plasticity in many brain regions, but the molecular mechanisms determining $\beta_1$AR subcellular localization are not fully understood. Using overlay and pull-down techniques, we found that the $\beta_1$AR carboxyl terminus associates with MAGI-2 (membrane-associated guanylate kinase inverted-2), a protein also known as S-SCAM (synaptic scaffolding molecule). MAGI-2 is a multidomain scaffolding protein that contains nine potential protein-protein interaction modules, including 6 PDZ domains, 2 WW domains, and a guanylate kinase-like domain. The $\beta_1$AR carboxyl terminus binds with high affinity to the first PDZ domain of MAGI-2, with the last few amino acids of the $\beta_1$AR carboxyl terminus being the key determinants of the interaction. In cells, the association of full-length $\beta_1$AR with MAGI-2 occurs constitutively and is enhanced by agonist stimulation of the receptor, as assessed by both co-immunoprecipitation experiments and immunofluorescence co-localization studies. Agonist-induced internalization of the $\beta_1$AR is markedly increased by co-expression with MAGI-2. Strikingly, this result is the opposite of the effect of co-expression with PSD-95, a previously reported binding partner of the $\beta_1$AR. Further cellular experiments revealed that MAGI-2 has no effect on $\beta_1$AR oligomerization but does promote association of $\beta_1$AR with the cytoplasmic signaling protein $\beta$-catenin, a known MAGI-2 binding partner. These data reveal that MAGI-2 is a specific $\beta_1$AR binding partner that modulates $\beta_1$AR function and facilitates the physical association of the $\beta_1$AR with intracellular proteins involved in signal transduction and synaptic regulation.**

Norepinephrine is a potent regulator of synaptic plasticity. For example, long-term potentiation of synaptic responses, a phenomenon believed to underlie some forms of long-lasting memory, is greatly promoted by noradrenergic stimulation in a number of brain regions (1–11). The effects of norepinephrine on synaptic plasticity are mediated largely through activation of the $\beta_1$-adrenergic receptor ($\beta_1$AR),[1] since mice lacking $\beta_1$AR fail to exhibit regulation of long-term potentiation by adrenergic stimulation (9). Pharmacological blockade of brain $\beta_1$-adrenergic receptors not only hinders the development of synaptic plasticity, it is also known to impair memory formation (12–17), thus underscoring the physiological importance of $\beta_1$AR regulation of synaptic processes.

The family of $\beta$-adrenergic receptors includes three subtypes, $\beta_1$AR, $\beta_2$AR, and $\beta_3$AR, with $\beta_1$AR and $\beta_2$AR being the subtypes found most abundantly in the brain. $\beta_2$-Adrenergic receptors in the central nervous system are expressed mainly in glia (18–20). In contrast, $\beta_1$-adrenergic receptors are found primarily in neurons and are particularly concentrated at synaptic junctions (18, 19, 21, 22). The synaptic localization of the $\beta_1$AR in the brain is believed to be important for the aforementioned modulation of synaptic plasticity by $\beta_1$-adrenergic receptors (1–11), and it is therefore a point of major interest to understand the mechanisms controlling $\beta_1$AR subcellular trafficking in neurons.

Synaptic targeting of receptors and channels in the brain can often be promoted by association of the receptors and channels with specific scaffolding proteins (23). It was recently reported that the $\beta_1$AR can associate with the synaptic scaffolding protein PSD-95 (24). PSD-95 contains three PDZ domains, which are conserved modules of ~90 amino acids that mediate association with specific motifs on the carboxyl termini of target proteins (25). The third PDZ domain of PSD-95 specifically associates with the carboxyl terminus of the $\beta_1$AR, and this interaction promotes the physical linkage of the $\beta_1$AR to other PSD-95-associated synaptic proteins such as *N*-methyl-*D*-aspartate-type glutamate receptors and also regulates $\beta_1$AR internalization (24).

While the interaction of $\beta_1$AR and PSD-95 is likely to be physiological important for $\beta_1$AR subcellular targeting *in vivo*,

* This work was supported National Institutes of Health Grants RO1-GM60982 (to R. A. H.) and RO1-NS34172 (to C. A. R.). The costs of publication of this article were defrayed in part by the payment of page charges. This article must therefore be hereby marked "*advertisement*" in accordance with 18 U.S.C. Section 1734 solely to indicate this fact.

§ Present address: University of Sheffield, Academic Neurology Unit, Sheffield, United Kingdom.

¶ To whom correspondence should be addressed: Dept. of Pharmacology, Emory University School of Medicine, 5113 Rollins Research Center, 1510 Clifton Rd., Atlanta, GA 30322. Tel.: 404-727-3699; Fax: 404-727-0365; E-mail: rhall@pharm.emory.edu.

[1] The abbreviations used are: $\beta_1$AR, $\beta_1$-adrenergic receptor; PDZ, PSD-95/Discs-large/ZO-1 homology; MAGI, membrane-associated guanylate kinase-like protein with an inverted domain structure; PSD-95, post-synaptic density protein of 95 kDa; S-SCAM, synaptic scaffolding molecule; NHERF, $Na^+/H^+$ exchanger regulatory factor; mNET1, murine neuroepithelial cell transforming gene 1; nRapGEP, neural Rap GDP/GTP exchange protein; CRIPT, cysteine-rich interactor of PDZ three; PTEN, phosphatase and tensin homolog deleted on chromosome 10; PCR, polymerase chain reaction; GST, glutathione *S*-transferase; CT, carboxyl terminus; His, hexahistidine-tagged; PAGE, polyacrylamide gel electrophoresis; WT, wild-type; HA, hemagglutinin; HEK, human embryonic kidney; PBS, phosphate-buffered saline; $BS^3$, bis(sulfosuccinimidyl)suberate.

it should be noted that the distributions of $\beta_1$AR (26–28) and PSD-95 (29–31) are not identical. There are a number of cellular populations where $\beta_1$AR is known to be highly expressed but PSD-95 is not detectable. The potential determinants of $\beta_1$AR targeting in neurons or other cells not expressing PSD-95 are unknown. We have identified another PDZ domain-containing scaffolding protein, MAGI-2 (membrane-associated guanylate kinase inverted-2) (32), a protein also known as S-SCAM (synaptic scaffolding molecule), as a high-affinity cellular binding partner of the $\beta_1$AR. While MAGI-2 and PSD-95 are structurally related PDZ proteins, we have found that they exhibit diametrically opposed effects on $\beta_1$AR internalization: MAGI-2 strongly promotes $\beta_1$AR internalization, whereas PSD-95 markedly inhibits it. The studies reported here describe the interaction of $\beta_1$AR with MAGI-2, and furthermore, describe the structural determinants of this interaction and its effects on $\beta_1$AR function.

## EXPERIMENTAL PROCEDURES

*Plasmids and Antibodies*—Mammalian expression plasmids pcDNA3/Flag-$\beta_1$AR and pcDNA3/Flag-$\beta_2$AR were described before (24). The mammalian expression plasmid for pCMV/HA-$\beta_1$AR was kindly provided by Hitoshi Kurose (University of Tokyo). To express GST fusion proteins of receptor carboxyl termini, $\beta_1$AR-CT (the carboxyl-terminal 100 amino acids of the human $\beta_1$AR), $\beta_2$AR-CT (the carboxyl-terminal 80 amino acids of the human $\beta_2$AR), and $\alpha_{1A}$AR-CT (the carboxyl-terminal 136 amino acids of the human $\alpha_{1A}$AR, prepared from a cDNA provided by Kenneth Minneman, Emory University) were amplified by PCR and then subcloned into pGEX-4T1 using the *Eco*RI and *Xho*I restriction sites. Point mutations of the $\beta_1$AR-CT were introduced by PCR and verified by ABI sequencing.

The MAGI-2 PDZ1, PDZ2, PDZ3, PDZ4, and PDZ5 constructs were prepared via PCR from a human MAGI-2/AIP1 cDNA (32). The MAGI-2 PDZ1 (corresponding to amino acids 420 through 559 of human MAGI-2), PDZ2 (599–743), PDZ3 (772–911), PDZ4 (915–1049), and PDZ5 (1140–1265) were inserted into the pET30A vector (Novagen) at the *Eco*RI and *Xho*I sites. The PDZ1 domain of MAGI-1/AIP3 (32) (corresponding to amino acids 446–571 of human MAGI-1) was also prepared via PCR and inserted into pET30A for expression as a hexahistidine-tagged and S-tagged fusion protein. The PSD-95 "PDZ1+2" and "PDZ3" constructs were prepared via PCR from a rat PSD-95 cDNA kindly provided by Morgan Sheng (Harvard Medical School). The PDZ1+2 (corresponding to amino acids 59–303 of rat PSD-95) and PDZ3 (corresponding to amino acids 307–446) were inserted into pET30A using *Eco*RI and *Xho*I sites introduced during PCR. The nNOS PDZ domain (corresponding to amino acids 1–150, prepared from a rat nNOS cDNA kindly provided by Thomas Michel, Harvard Medical School) was also prepared via PCR and inserted into pET30A at the *Eco*RI and *Xho*I sites. The NHERF-1 PDZ domain constructs in pET30A have been described previously (33, 34).

Monoclonal anti-GST antibody and polyclonal anti-His antibody were from Santa Cruz. Monoclonal anti-hemagglutinin (HA) 12CA5 antibody was from Roche Molecular Biochemicals. Anti-$\beta$-catenin antibody was purchased from Transduction Laboratories (Lexington, KY). Anti-Flag M2 antibody and anti-Flag M2 affinity gel were from Sigma. Horseradish peroxidase-conjugated anti-mouse IgG and anti-rabbit IgG secondary antibodies were from Amersham Pharmacia Biotech.

*Cell Culture and Transfection*—All tissue culture media and related reagents were purchased from Life Technologies, Inc. HEK-293 cells were maintained in complete medium (minimal essential medium plus 10% fetal bovine serum and 1% penicillin/streptomycin) in a 37 °C, 5% $CO_2$ incubator. For transient transfection, 2 $\mu$g of total DNA was mixed with LipofectAMINE (Life Technologies, Inc.) and added to 5 ml of serum-free medium in 100-mm tissue culture plates containing HEK-293 cells at ~50–80% confluency. Following a 3-h incubation, 6 ml of complete medium was added. Twenty-four hours later, the medium was replaced with fresh complete medium, and the cells were incubated for an additional 24–48 h before harvesting. Whole cell extracts were prepared by lysing cells in 1 ml of lysis buffer (20 mM HEPES, 150 mM NaCl, 2 mM EDTA, 2 mM benzamidine, 1% Triton X-100) on ice for 30 min. The lysates were clarified by centrifugation at 21,000 × *g* for 12 min at 4 °C. The clarified supernatants were then used in all following *in vitro* GST pull-down or cellular co-immunoprecipitation experiments. 50 $\mu$l of such supernatant was diluted into equal amount 3 times sample buffer and served as whole cell extract.

*Western Blotting*—Samples (5–10 $\mu$g/lane) were run on 4–20% SDS-PAGE gels (Novex, San Diego) for 1 h at 150 V and then transferred to pure nitrocellulose. The blots were blocked in a buffer consisting of 2% milk, 0.1% Tween-20 in PBS ("blot buffer") for 1 h at room temperature and subsequently incubated with primary antibody in blot buffer for 1 h at room temperature. The blots were then washed three times with blot buffer and incubated for 1 h at room temperature with a horseradish peroxidase-conjugated secondary antibody in blot buffer. Following three final washes with blot buffer and one wash with PBS, bands were visualized via chemiluminescence with the ECL kit from Amersham Pharmacia Biotech.

*Pull-down Assays*—GST fusion proteins were purified on glutathione-agarose beads. Aliquots of the fusion protein/bead mixture in 1.5-ml microcentrifuge tubes were blocked for 1 h with 1 ml of a 3% bovine serum albumin buffer (containing 10 mM HEPES, 50 mM NaCl, and 0.1% Tween 20) on ice for 30 min. Equal concentrations of various His/S-tagged fusion proteins were then incubated with the beads in 1 ml of the 3% bovine serum albumin blocking buffer at 4 °C with end-over-end rotation for 1 h. The beads were washed five times with ice-cold 3% bovine serum albumin blocking buffer and washed once with harvest buffer (20 mM HEPES, 150 mM NaCl, 2 mM EDTA, 2 mM benzamidine, 1% Triton X-100). The proteins were eluted from the beads with 1 × SDS-PAGE sample buffer, resolved via SDS-PAGE, and transferred to nitrocellulose. The His-tagged fusion proteins were detected via Western blotting with S-protein horseradish peroxidase conjugate from Novagen (1:4000), and bands were visualized via chemiluminescence. For experiments involving pull-downs from cell lysates, the procedure was the same except that pulled-down proteins were detected on the Western blot using appropriate antibodies (*e.g.* anti-$\beta$-catenin antibodies to detect pulled-down $\beta$-catenin).

*Immunoprecipitation*—Cells were harvested and lysed in 500 $\mu$l of ice-cold lysis buffer (10 mM HEPES, 50 mM NaCl, 5 mM EDTA, 1 mM benzamidine, 0.5% Triton X-100). The lysate was solubilized via end-over-end rotation at 4 °C for 30 min and clarified via centrifugation at 14,000 rpm for 15 min. A small fraction of the supernatant was taken at this point and incubated with SDS-PAGE sample buffer in order to examine expression of proteins in the whole cell extract. The remaining supernatant was incubated with 30 $\mu$l of anti-Flag M2 affinity gel (Sigma) for 2 h with end-over-end rotation at 4 °C. After five washes with 1.0 ml of lysis buffer, the immunoprecipitated proteins were eluted from the beads with 1 × SDS-PAGE sample buffer, resolved by SDS-PAGE, and subjected to Western blot analysis with appropriate antibodies.

*Overlay Assay*—The binding of receptor carboxyl terminus GST fusion proteins to His/S-tagged PDZ domain fusion proteins was assayed via a blot overlay technique. The His/S-tagged PDZ domains (2 $\mu$g/lane) were run on 4–20% SDS-PAGE gels (Novex, San Diego), blotted, and overlaid with the receptor CT-GST fusion proteins (50 nM final concentration) in a buffer consisting of 2% milk, 0.1% Tween 20 in PBS (blot buffer) for 1 h at room temperature. The blots were then washed three times with blot buffer and incubated for 1 h at room temperature with a monoclonal anti-GST antibody. The blots were then washed again three times with blot buffer and incubated for 1 h at room temperature with a horseradish peroxidase-conjugated anti-mouse IgG secondary antibody in blot buffer. Following three final washes with blot buffer, the binding of the GST fusion proteins was visualized via chemiluminescence as described above. In the reverse experiments, the GST fusion proteins were run on SDS-PAGE gels, transferred to nitrocellulose, and then overlaid with the His/S-tagged PDZ domains in blot buffer. For these experiments, the bound His/S-tagged proteins were detected via incubation of the blots with S protein horseradish peroxidase conjugate (1:4000) followed by chemiluminescence.

*Receptor Internalization*—Receptor internalization was assayed using a previously described method (35). Briefly, HEK-293 cells in 100-mm dishes were transiently transfected with pcDNA3/Flag-$\beta_1$AR in the absence and presence of pcDNA3/HA-MAGI-2. One day after transfection, cells were split into new dishes and grown overnight at 37 °C. On the second day, cells were treated with 50 $\mu$M isoproterenol for 10 min. Cells were then immediately washed with PBS twice, placed at 4 °C, and incubated with 1 mg/ml of the membrane-impermeable cross-linking reagent $BS^3$ 30 min. After washing the cells with PBS containing Tris (to quench any residual cross-linker), the cells were harvested in lysis buffer (20 mM HEPES, 150 mM NaCl, 2 mM EDTA, 2 mM benzamidine, 1% Triton X-100). Cell lysates were resolved on SDS-PAGE. Flag-tagged receptors were visualized via Western blot with an anti-Flag M2 Ab followed by an horseradish peroxidase-conjugated anti-mouse IgG Ab as described above. Bands for cross-linked-$\beta_1$AR (high-molecular band, representing surface receptor) and non-cross-

linked-$\beta_1$AR (56 kDa, representing receptor not on the surface) were visualized via chemiluminescence and quantified using a densitometer. Multiple control experiments revealed that intracellular proteins, such as actin and tubulin, were not cross-linked by the $BS^3$ treatment, indicating that the $BS^3$ was acting only on surface-expressed transmembrane proteins (actin and tubulin were both detected on the blots with antibodies from Sigma). Receptor internalization was defined as the percentage reduction in surface receptors following agonist stimulation, relative to matched control cells that were not stimulated with isoproterenol.

*Immunofluorescence Microscopy*—HEK-293 cells were transiently transfected with pcDNA3/Flag-$\beta_1$AR and/or pcDNA3/HA-MAGI-2. Forty-eight hours after transfection, cells were washed three times with Dulbecco's PBS and then incubated for 10 min at 37 °C in the absence or presence of 50 $\mu$M isoproterenol. Following this incubation, cells were fixed in 4% paraformaldehyde in PBS for 30 min at room temperature. To visualize the subcellular localization of $\beta_1$AR and MAGI-2, cells were blocked and permeabilized with a buffer containing 2% bovine serum albumin and 0.04% saponin ("saponin buffer") for 30 min at room temperature. The cells were then incubated with anti-Flag M2 monoclonal Ab (Sigma) at a 1:500 dilution and/or a rabbit polyclonal anti-MAGI-2 Ab (36) at a 1:500 dilution for 1 h at room temperature. After three washes (1 min) with saponin buffer, the cells were incubated with a Texas Red-conjugated anti-mouse IgG Ab (1:200) and/or a fluorescein isothiocyanate-conjugated anti-rabbit IgG (1:200) for 1 h at room temperature. After three washes (1 min) with saponin buffer and one wash with PBS, coverslips were mounted and Texas Red-labeled receptors and fluorescein isothiocyanate-labeled MAGI-2 were visualized with a Zeiss LSM-410 laser confocal microscope. Multiple control experiments, utilizing either transfected cells in the absence of primary antibody or untransfected cells in the presence of primary antibody, revealed a very low level of background staining, indicating that the primary antibody-dependent immunostaining observed in the transfected cells was specific.

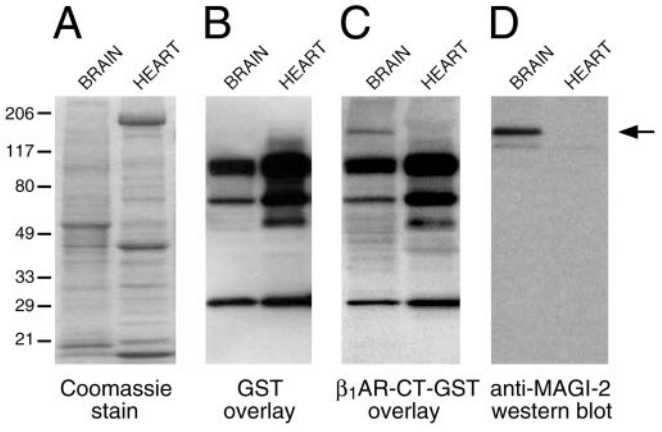


FIG. 1. **Identification of a $\beta_1$AR-CT binding partner that corresponds in size to MAGI-2.** *A,* lysates from brain and heart tissue were run on a 4–20% SDS-PAGE and Coomassie stained to visualize all proteins. *B,* the same samples were also transferred to nitrocellulose and overlaid with 50 nM GST, which did not bind specifically to any proteins in the lysates. Several immunoreactive bands were evident in both the brain and heart lanes, but these proteins were also detected in anti-GST Western blots even when the blots were not first overlaid with GST (data not shown). *C,* $\beta_1$AR-CT-GST binds specifically to a 170-kDa protein found in brain. Overlays with 50 nM $\beta_1$AR-CT-GST and subsequent Western blotting to detect GST revealed a specifically labeled band at 170 kDa in addition to the nonspecific bands that were also detected in the control GST overlay. *D,* the $\beta_1$AR-CT binding partner matches MAGI-2 in size. Western blots with an anti-MAGI-2 antibody revealed that the major immunoreactive band is 170 kDa in size and found specifically in brain, consistent with the properties of the $\beta_1$AR-CT binding partner.

## RESULTS

In order to identify potential cytoplasmic binding partners of the $\beta_1$-adrenergic receptor, the carboxyl terminus of the human $\beta_1$-adrenergic receptor ($\beta_1$AR-CT) was prepared as a GST fusion protein and utilized in blot overlay studies of brain and heart tissue, two areas where $\beta_1$AR is abundantly expressed. These studies were carried out in conjunction with yeast two-hybrid screens of a brain cDNA library utilizing the $\beta_1$AR-CT as bait. The yeast two-hybrid screens, as previously described (24), yielded two interacting clones corresponding to overlapping regions of PSD-95, a brain-specific protein of 95 kDa. In contrast, the blot overlay studies with the $\beta_1$AR-CT-GST revealed a single major interacting band at ~170 kDa (Fig. 1). This band was detected in brain but not heart (Fig. 1*C*), and was not detected by overlays with GST alone (Fig. 1*B*). The GST moiety of the $\beta_1$AR-CT-GST fusion protein bound nonspecifically to several bands in the heart and brain lysates, however, including a band in the range of 95–100 kDa. This nonspecific GST-binding band made it difficult to assess whether the $\beta_1$AR-CT-GST might be associating with a 95-kDa species in the brain lysate corresponding to PSD-95. Nonetheless, the 170-kDa band detected specifically by the $\beta_1$AR-CT-GST in the brain was clearly too large to correspond to PSD-95, and thus we set out to identify this protein.

The $\beta_1$AR-CT interacts with PSD-95 via the PDZ3 domain of PSD-95 (24). Reasoning that the $\beta_1$AR-CT interacting protein observed in our blot overlays might exhibit structural similarity to this domain, we performed BLAST searches with the protein sequence of PSD-95 PDZ3. These searches revealed a list of several dozen proteins exhibiting significant homology to PSD-95 PDZ3, but the vast majority of these matches were proteins of less than 100 kDa in size. The only protein on the list that matched the size of the $\beta_1$AR-CT-interacting protein seen in our blot overlays was MAGI-2, a 170-kDa brain-specific protein that contains several PDZ domains with significant similarity to PSD-95 PDZ3. We therefore probed our samples of the heart and brain lysate with an anti-MAGI-2 antibody (36) and compared the results to those from the $\beta_1$AR-CT-GST overlays. As shown in Fig. 1*D*, the anti-MAGI-2 antibody recognizes a major band of ~170 kDa in the brain tissue, and this band matches up precisely in size with the $\beta_1$AR-CT interacting protein observed in our overlay experiments.

We next directly tested the potential interaction of MAGI-2 with the $\beta_1$AR-CT using purified fusion proteins. His-tagged fusion proteins corresponding to PDZ1–5 of MAGI-2 were purified and examined in blot overlay experiments for binding to the $\beta_1$AR-CT-GST. As shown in Fig. 2*A*, the $\beta_1$AR-CT-GST bound robustly to PDZ1 and weakly or not at all to the other four PDZ domains. When probed against a panel of various PDZ domains, the $\beta_1$AR-CT-GST bound not only to the first PDZ domain of MAGI-2, but also to the first PDZ domain of a related protein, MAGI-1, and also to the third PDZ domain of PSD-95 (Fig. 2*B, upper panel*). The binding of the $\beta_1$AR-CT-GST to the MAGI-2 PDZ1 domain was comparable to the binding of the $\beta_1$AR-CT-GST to PSD-95 PDZ3. No binding of the $\beta_1$AR-CT-GST was observed to PSD95 PDZ1+2, nor to the PDZ domains of NHERF-1 or nNOS, demonstrating the specificity of interaction between the $\beta_1$AR-CT-GST and the MAGI PDZ1 and PSD-95 PDZ3 domains. In contrast to the $\beta_1$AR-CT-GST, the $\beta_2$AR-CT-GST did not bind at all to any of the MAGI or PSD-95 PDZ domains (Fig. 2*B, lower panel*), but rather bound specifically to PDZ1 of NHERF-1, as previously reported (33, 34).

In the reverse overlay experiments, where the His-tagged MAGI-2 PDZ domains were overlaid onto blotted samples of the $\beta_1$AR-CT-GST and $\beta_2$AR-CT-GST, strong binding of PDZ1 to the $\beta_1$AR-CT was observed (Fig. 2*C*), but no binding of the other MAGI-2 PDZ domains to the $\beta_1$AR-CT-GST could be detected (data not shown). Moreover, no binding of MAGI-2 PDZ1 to the $\beta_2$AR-CT-GST or $\alpha_{1A}$AR-CT-GST was observed, further demonstrating the specificity of the interaction of MAGI-2 PDZ1 with $\beta_1$AR. Saturation binding studies using the blot overlay technique yielded an estimated binding affinity of

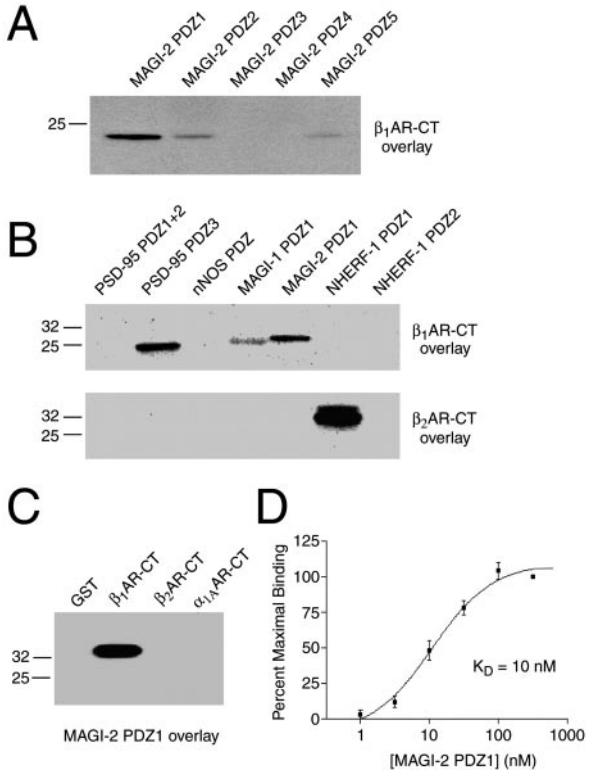


FIG. 2. **The $\beta_1$AR-CT binds specifically and with high affinity to the PDZ1 domain of MAGI-2.** *A,* $\beta_1$AR-CT binds preferentially to PDZ1 of MAGI-2. Equal amounts (2 $\mu$g) of purified His-tagged fusion proteins corresponding to PDZ domains 1–5 of MAGI-2 were run on a 4–20% SDS-PAGE gel and transferred to nitrocellulose. Overlay of the blot with $\beta_1$AR-CT-GST (25 nM) revealed strong binding to PDZ1, weak binding to PDZ2 and PDZ5, and no detectable binding to PDZ3 and PDZ4. *B,* $\beta_1$AR-CT binds as well to MAGI-2 PDZ1 as to PSD-95 PDZ3. Equal amounts (2 $\mu$g) of purified His-tagged fusion proteins corresponding to PDZ domains from PSD-95, nNOS, MAGI-1, MAGI-2, and NHERF-1 were run on a 4–20% SDS-PAGE gel and transferred to nitrocellulose. Overlays with $\beta_1$AR-CT-GST (25 nM) revealed strong binding to PSD-95 PDZ3 and MAGI-2 PDZ1, moderate binding to MAGI-1 PDZ1, and no detectable binding to the first two PDZ domains of PSD-95 or PDZ domains of nNOS or NHERF-1. In contrast, overlays with $\beta_2$AR-CT-GST (25 nM) revealed strong binding to NHERF-1 PDZ1 but no detectable binding to any of the other PDZ domains examined. *C,* MAGI-2 PDZ1 binds specifically to $\beta_1$AR-CT. In the reverse of the overlay experiments described in the first two panels of this figure, equal amounts (2 $\mu$g) of purified GST fusion proteins corresponding to the carboxyl termini of various adrenergic receptor subtypes were run on an SDS-PAGE gel and transferred to nitrocellulose. Overlay with His/S-tagged MAGI-2 PDZ1 (20 nM) revealed strong binding to $\beta_1$AR-CT-GST but no detectable binding to control GST, $\beta_2$AR-CT-GST, or $\alpha_1$AR-CT-GST. The data shown here, as well as those shown in the first two panels of this figure, are representative of three to five independent experiments each. Molecular mass standards (in kDa) are indicated on the *left*. *D,* the interaction between $\beta_1$AR-CT and MAGI-2 PDZ1 is of high affinity. Nitrocellulose strips containing 2 $\mu$g of $\beta_1$AR-CT-GST (equivalent to *lane 2* in the preceding panel) were incubated with His/S-tagged MAGI-2 PDZ1 at 6 concentrations between 1 and 300 nM. Specific binding of MAGI-2 PDZ1 did not increase between 100 and 300 nM, and thus the binding observed at 300 nM was defined as "maximal" binding. The binding observed at the other concentrations was expressed as a percentage of maximal binding within each experiment. The *bars* and *error bars* shown on this graph indicate mean ± S.E. ($n$ = 3). The $K_D$ for MAGI-2 PDZ1 binding to $\beta_1$AR-CT was estimated at 10 nM.

10 nM for the interaction of MAGI-2 PDZ1 with the $\beta_1$AR-CT (Fig. 2*D*).

In order to explore the structural determinants of the $\beta_1$AR-CT/MAGI-2 PDZ1 association, we prepared a number of point mutations of the $\beta_1$AR-CT as GST fusion proteins. The binding of His-tagged MAGI-2 PDZ1 to these point mutants is shown in Fig. 3*A*. The last five amino acids of the wild-type $\beta_1$AR-CT are SESKV. Mutation of the terminal valine residue to alanine

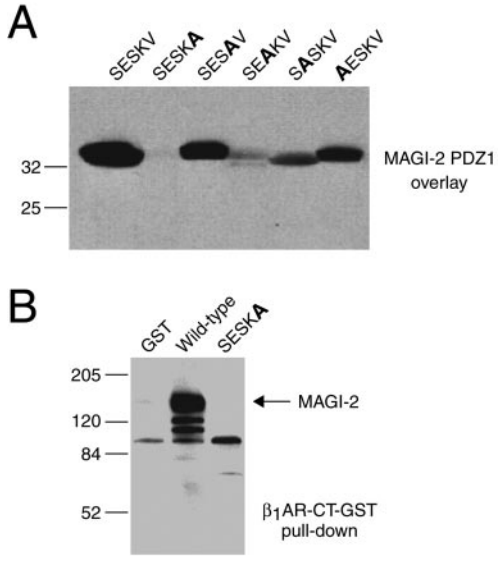


FIG. 3. **The last few amino acids of the $\beta_1$AR-CT are the key determinants for interaction with MAGI-2.** *A,* mutations to alanine at positions 0, −2, and −3 of the $\beta_1$AR-CT inhibit binding to MAGI-2 PDZ1. Purified GST fusion proteins (2 $\mu$g) corresponding to either the wild-type $\beta_1$AR-CT (denoted by its last five amino acids, "SESKV") or a point-mutated version of the $\beta_1$AR-CT (denoted by sequential replacement of each of the last five amino acids with alanine) were run on a 4–20% SDS-PAGE gel and transferred to nitrocellulose. Overlay of the blot with His/S-tagged MAGI-2 PDZ1 (20 nM) revealed strong binding to the wild-type $\beta_1$AR-CT as well as to the mutant versions of the $\beta_1$AR-CT with substitutions to alanine at −1 and −4. The valine-to-alanine mutation at the terminal position, however, almost completely blocked the binding of MAGI-2 PDZ1, while mutations to alanine at −2 and −3 also substantially inhibited the $\beta_1$AR-CT/MAGI-2 PDZ1 interaction. *B,* mutation of the last amino acid of the $\beta_1$AR-CT blocks association with full-length MAGI-2. Purified fusion proteins corresponding to GST alone (*lane 1*), $\beta_1$AR-CT-GST wild-type (*lane 2*), and a $\beta_1$AR-CT point mutant with the terminal valine changed to alanine ("SESKA"; *lane 3*) were adsorbed to glutathione-agarose beads and used to pull-down full-length MAGI-2 from lysates prepared from HEK-293 cells transfected with HA-tagged MAGI-2. The pulled down MAGI-2 was detected with an anti-HA (12CA5) antibody via Western blot. MAGI-2 was robustly pulled down by the wild-type $\beta_1$AR-CT-GST, but no detectable MAGI-2 was pulled down with either control GST or the $\beta_1$AR-CT-GST point mutant, indicating that the last amino acid of the $\beta_1$AR is critical for association with MAGI-2. The data shown in both panels of this figure are representative of three to four independent experiments, and molecular mass standards (in kDa) are shown on the *left* of each panel.

completely blocked interaction of the $\beta_1$AR-CT with MAGI-2 PDZ1. In contrast, mutation of the lysine residue at the −1 position to alanine had little effect on binding of MAGI-2 PDZ1. Mutations to alanine at the −2 and −3 positions of the $\beta_1$AR-CT significantly reduced binding of MAGI-2 PDZ1, whereas a Ser to Ala mutation at −4 had little effect. Thus, three of the final four amino acids of the $\beta_1$AR (positions 0, −2, and −3) are the primary determinants of binding to MAGI-2 PDZ1. Since the terminal valine was found to be the most critical residue for the interaction, we examined the binding of the wild-type $\beta_1$AR-CT (SESKV) and the SESKA mutant to full-length MAGI-2 from lysates derived from HEK-293 cells transfected with HA-MAGI-2. As shown in Fig. 3*B*, wild-type $\beta_1$AR-CT was able to pull-down a large amount of full-length MAGI-2 from the lysates, whereas no detectable MAGI-2 was pulled down by the SESKA point mutant.

We next examined the interaction of full-length $\beta_1$AR with MAGI-2 in a cellular context. HEK-293 cells were transfected with Flag-$\beta_1$AR and His-tagged MAGI-2 PDZ1, and co-immunoprecipitation of the two proteins was examined in the absence and presence of agonist stimulation (Fig. 4). Under basal conditions, a significant amount of MAGI-2 PDZ1 could be co-immunoprecipitated with the Flag-$\beta_1$AR. Following a 10-

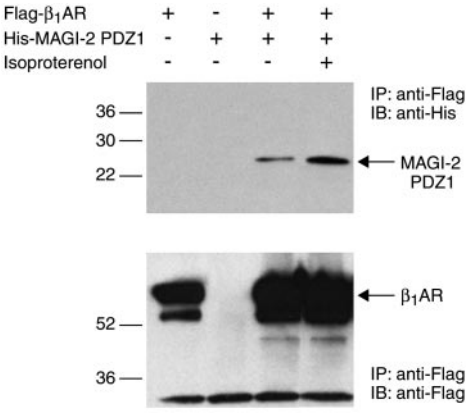


FIG. 4. **Co-immunoprecipitation of MAGI-2 PDZ1 with full-length $\beta_1$AR is enhanced by agonist stimulation.** HEK-293 cells transfected with Flag-$\beta_1$AR (*lane 1*), His-MAGI-2 PDZ1 (*lane 2*), or Flag-$\beta_1$AR and His-MAGI-2 PDZ1 together (*lanes 3* and *4*) were solubilized and incubated with anti-Flag antibody coupled to beads in order to immunoprecipitate the Flag-tagged receptor. As shown in the *bottom panel*, immunoprecipitation of the Flag-$\beta_1$AR was successful and fairly even between the different samples. Co-immunoprecipitation of MAGI-2 PDZ1 (*top panel*) was evident under basal conditions (*lane 3*) and was consistently enhanced in samples where the cells had been stimulated with 10 $\mu$M isoproterenol for 10 min prior to solubilization. These data are representative of four independent experiments. Molecular mass standards (in kDa) are shown on the *left*.

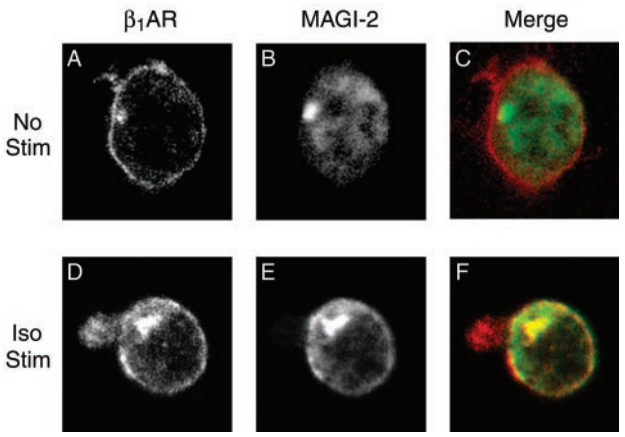


FIG. 5. **Immunofluorescence co-localization of $\beta_1$AR and MAGI-2 in cells.** Flag-$\beta_1$AR and HA-MAGI-2 were co-expressed in HEK-293 cells and visualized via immunofluorescence. Under basal conditions, $\beta_1$AR-CT immunostaining was mainly localized to the plasma membrane (*panel A*), while MAGI-2 was found both at the plasma membrane and in the cytoplasm (*panel B*). Merging of these two images (*panel C*), with the $\beta_1$AR immunostaining shown in *red* and the MAGI-2 staining shown in *green*, yielded a significant but not striking degree of co-localization. When cells were stimulated with isoproterenol (50 $\mu$M) for 10 min prior to fixation, $\beta_1$AR immunostaining was still found predominantly at the cell surface (*panel D*), although more $\beta_1$AR could be detected in the cytoplasm, presumably due to receptor internalization. MAGI-2 immunostaining was still found both at the plasma membrane and in the cytoplasm (*panel E*), but the plasma membrane immunostaining was much more pronounced following agonist stimulation than under basal conditions, leading to a higher degree of $\beta_1$AR/MAGI-2 co-localization (*panel F*). These data are representative of six independent experiments.

min stimulation with the selective $\beta$-adrenergic receptor agonist isoproterenol, the amount of co-immunoprecipitated MAGI-2 PDZ1 was consistently increased. Quantification of the immunoprecipitation results revealed that the amount of MAGI-2 PDZ-1 co-immunoprecipitated in the presence of isoproterenol stimulation was 260% of the amount co-immunoprecipitated under basal conditions. These data reveal that the $\beta_1$AR associates constitutively in cells with the first PDZ domain of MAGI-2, and that the interaction can be promoted (or perhaps stabilized) by agonist activation of the $\beta_1$AR.

The interaction of full-length MAGI-2 with full-length $\beta_1$AR in cells was next examined via immunofluorescence microscopy. HEK-293 cells were transfected with both $\beta_1$AR and MAGI-2, and immunostaining for both proteins was analyzed in the absence and presence of isoproterenol stimulation. Immunostaining for $\beta_1$AR was localized primarily to the plasma membrane under basal conditions (Fig. 5*A*), whereas MAGI-2 immunostaining was found diffusely spread throughout the cytoplasm and along the plasma membrane (Fig. 5*B*). A significant but not striking overlap of $\beta_1$AR and MAGI-2 immunostaining was consistently observed under basal conditions (Fig. 5*C*). Following a 10-min stimulation with isoproterenol, $\beta_1$AR immunostaining was still found mainly along the plasma membrane, although significantly more $\beta_1$AR was observed in the cytoplasm, consistent with receptor internalization (Fig. 5*D*). MAGI-2 localization was even more significantly altered following isoproterenol stimulation, with a significant fraction of MAGI-2 now being found at the plasma membrane (Fig. 5*E*), where it was much more clearly co-localized with $\beta_1$AR immunostaining than under basal conditions (Fig. 5*F*).

We next sought to understand the functional importance of the $\beta_1$AR/MAGI-2 interaction. Experiments examining cyclic AMP generation induced by isoproterenol stimulation of $\beta_1$AR expressed in HEK-293 cells revealed no significant difference in $EC_{50}$ between cells in which the $\beta_1$AR was expressed alone and cells in which the $\beta_1$AR was co-expressed with MAGI-2 (data not shown). These observations are similar to previous findings that PSD-95 co-expression does not alter cyclic AMP generation induced by $\beta_1$AR stimulation (24). Since the interaction of $\beta_1$AR with PSD-95 was previously shown to inhibit $\beta_1$AR internalization (24), we studied the agonist-induced internalization of the $\beta_1$AR expressed in HEK-293 cells in the absence and presence of PSD-95 and MAGI-2 co-expression. As shown in Fig. 6, a 10-min stimulation with isoproterenol resulted in ~14% internalization of the $\beta_1$AR. In the presence of PSD-95 co-expression, $\beta_1$AR internalization was markedly reduced, consistent with previous findings (24). Co-expression of MAGI-2, however, had the opposite effect of PSD-95 co-expression, promoting $\beta_1$AR internalization by nearly 3-fold.

Since MAGI-2 is believed to act primarily as a scaffolding protein to link together cellular signaling proteins, we explored whether MAGI-2 might be able to facilitate physical linkage between the $\beta_1$AR and another known MAGI binding partner. $\beta$-Catenin is known to bind to PDZ3 of MAGI-2 (37, 38), and we therefore performed pull-down studies examining the potential interaction of $\beta$-catenin with $\beta_1$AR-CT (Fig. 7*A*). In lysates prepared from untransfected cells, no $\beta$-catenin could be detected in association with the $\beta_1$AR-CT. In cells transfected with full-length MAGI-2, however, $\beta$-catenin robustly associated with the $\beta_1$AR-CT. These data indicate that MAGI-2 can act as a scaffold to physically link together two proteins, $\beta_1$AR and $\beta$-catenin, that bind to distinct MAGI-2 PDZ domains.

MAGI-2 is known to be capable of oligomerization (39), and we therefore wondered whether association with MAGI-2 might promote cellular oligomerization of the $\beta_1$AR. Many G protein-coupled receptors are known to oligomerize (40). The $\beta_2$-adrenergic receptor has been particularly intensively studied with regard to its oligomerization (41–43), but oligomerization of the $\beta_1$AR has not been reported. We studied $\beta_1$AR oligomerization via co-immunoprecipitation utilizing HEK-293 cells transfected with Flag-$\beta_1$AR and HA-$\beta_1$AR. As shown in Fig. 7*B*, control experiments revealed that HA-$\beta_1$AR expressed alone was not detectably immunoprecipitated by an anti-Flag antibody. However, when HA-$\beta_1$AR and Flag-$\beta_1$AR were expressed together, the anti-Flag antibody not only immunopre-

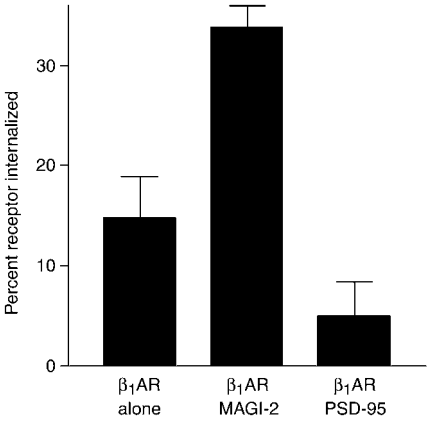


FIG. 6. **Agonist-induced $\beta_1$AR internalization is enhanced by co-expression of MAGI-2 but inhibited by co-expression of PSD-95.** HEK-293 cells were transfected with Flag-$\beta_1$AR alone or Flag-$\beta_1$AR in combination with either MAGI-2 or PSD-95. The cells were stimulated for 10 min with isoproterenol (10 $\mu$M) and the amount of receptor lost from the cell surface was quantified relative to unstimulated cells. Co-expression with MAGI-2 markedly promoted $\beta_1$AR internalization in response to the isoproterenol treatment, whereas co-expression with PSD-95 markedly decreased the amount of agonist-induced receptor internalization. The *bars* and *error bars* represent the mean ± S.E. for three independent experiments, each performed in duplicate.

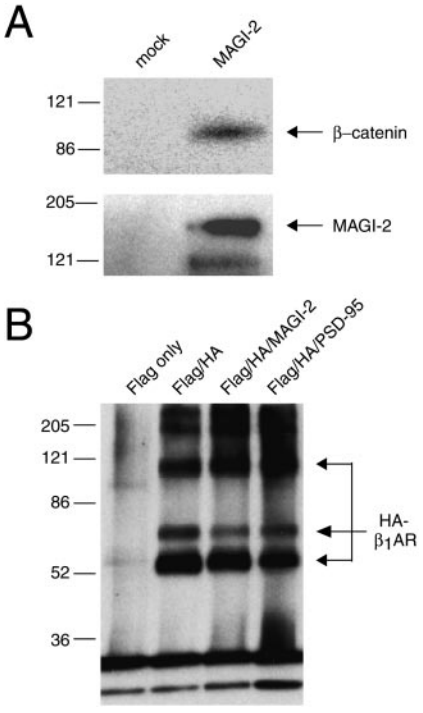


FIG. 7. **MAGI-2 promotes $\beta_1$AR association with $\beta$-catenin but does not promote $\beta_1$AR oligomerization.** *A,* MAGI-2-dependent association of $\beta$-catenin with $\beta_1$AR-CT. Lysates from either mock-transfected HEK-293 cells ("mock," *lane 1*) or cells transfected with MAGI-2 (*lane 2*) were incubated with glutathione-agarose beads loaded with $\beta_1$AR-CT-GST in order to perform pull-down assays. Endogenous $\beta$-catenin was pulled down by the $\beta_1$AR-CT from the MAGI-2-transfected cells but not from untransfected cells, suggesting that MAGI-2 facilitates physical linkage of the $\beta_1$AR-CT to $\beta$-catenin. *B,* $\beta_1$-adrenergic receptors form oligomers in cells, and the extent of $\beta_1$AR oligomerization is not enhanced by co-expression of either MAGI-2 or PSD-95. HEK-293 cells were transfected with Flag-$\beta_1$AR alone ("Flag only," *lane 1*), Flag-$\beta_1$AR plus HA-$\beta_1$AR ("Flag/HA," *lane 2*), Flag-$\beta_1$AR/HA-$\beta_1$AR/MAGI-2 (*lane 3*), or Flag-$\beta_1$AR/HA-$\beta_1$AR/PSD-95 (*lane 4*). The cells were solubilized and incubated with anti-Flag antibody to immunoprecipitate the Flag-tagged $\beta_1$AR. Western blots were then performed to detect any co-immunoprecipitated HA-tagged $\beta_1$AR, which runs as doublet in the range of 56–62 kDa in addition to higher molecular mass bands that presumably represent $\beta_1$AR complexes incompletely dissociated by the SDS-PAGE sample buffer. Co-immunoprecipitation of HA-$\beta_1$AR with Flag-$\beta_1$AR was clearly detected in all co-transfected samples (*lanes 2–4*), and the extent of co-immunoprecipitation was not significantly altered by co-expression of either MAGI-2 or PSD-95. Total expression of Flag-$\beta_1$AR and HA-$\beta_1$AR in the differentially transfected samples was comparable, as assessed in separate Western blots (not shown). These data, as well as those from the preceding panel, are representative of three to four independent experiments each. Molecular mass standards (in kDa) are shown on the *left* of each panel.

cipitated Flag-$\beta_1$AR, it also strongly co-immunoprecipitated HA-$\beta_1$AR. The amount of co-immunoprecipitation was unchanged when the two receptors were co-expressed with MAGI-2 or with PSD-95. These data suggest that the $\beta_1$AR is capable of homo-oligomerization in cells, and furthermore, suggest that the efficiency of $\beta_1$AR homo-oligomerization is not altered by association with either MAGI-2 or PSD-95.

## DISCUSSION

We have found that the carboxyl terminus of the $\beta_1$-adrenergic receptor binds with high affinity to the first PDZ domain of MAGI-2. This interaction was first detected in blot overlay studies, which were carried out in conjunction with extensive yeast two-hybrid screens using the $\beta_1$AR-CT as bait. The yeast two-hybrid screens identified PSD-95 as a high-affinity binding partner of the $\beta_1$AR-CT (24), while the biochemical approach described here resulted in the identification of MAGI-2 as a $\beta_1$AR binding partner. There are many diverse approaches that can be used in identifying intracellular proteins that interact with cell surface receptors (44). Since each approach has its own inherent strengths and weaknesses, it is often advantageous to utilize several approaches together. The multiple approaches that we have taken with the $\beta_1$AR-CT have resulted in the identification of two related proteins, PSD-95 and MAGI-2, which bind to the same determinants on the distal carboxyl terminus of the $\beta_1$AR but have quite distinct effects on $\beta_1$AR function.

PSD-95 and MAGI-2 are both scaffolding proteins, but they differ in terms of the set of intracellular proteins they are known to bind. The set of known PSD-95-binding proteins includes *N*-methyl-*D*-aspartate-type glutamate receptors (45), Kv1.4 potassium channels (46), neuronal nitric-oxide synthase (30), neuroligins (48), CRIPT (49), Citron (50, 51), Fyn (52), Cypin (53), and ErbB4 (54). In contrast, the set of proteins known to bind to MAGI-2 includes atrophin (32), *N*-methyl-*D*-aspartate-type glutamate receptors (55), neuroligins (55), $\delta$-catenin (37), $\beta$-catenin (37, 38), nRAP-GEP (57) and PTEN (36). MAGI-2 has two close relatives, MAGI-1 (58) and MAGI-3 (59), which have distinct tissue distributions. MAGI-3 has only recently been identified, but MAGI-1 is known to bind to a number of intracellular proteins, including atrophin (32), $\beta$-catenin (60), nRAP-GEP (61), the brain angiogenesis inhibitor (62), megalin (63), and mNET1 (64). In the experiments described in the present report, we found that the PDZ1 domains of MAGI-1 and MAGI-2 bind well to the $\beta_1$AR-CT; MAGI-3 is also a probable $\beta_1$AR binder as well given that its sequence is nearly identical to MAGI-1 and MAGI-2 in the PDZ1 region. Thus, the set of intracellular proteins to which the $\beta_1$AR in a given cell may be physically connected is likely to depend on whether the cell also expresses MAGI-1, MAGI-2, MAGI-3, PSD-95, or some combination of these proteins. $\beta_1$AR functional properties, such as the rate and extent of agonist-mediated receptor internalization (65–68), are known to differ markedly in different cell types, and the identification of $\beta_1$AR-interacting proteins with distinct tissue distributions is a key step toward understanding the effects of cellular context on $\beta_1$AR function.

PSD-95 and MAGI-2 differ not only in their set of associated intracellular proteins, but also in their effect on $\beta_1$AR internal-

ization. $\beta_1$AR internalization is markedly inhibited by association with PSD-95 (24) but markedly promoted by association with MAGI-2. This difference may arise from differential lipid modification of PSD-95 *versus* MAGI-2: PSD-95 is known to be palmitoylated (69) and strongly membrane-anchored (29, 69), whereas MAGI-2 is not known to be lipid-modified and is not strongly anchored to the plasma membrane (55). The palmitoylation of PSD-95, in fact, plays a critical role in its ability to inhibit the internalization of the Kv1.4 potassium channel (69), which is consistent with the idea that the differential lipid modification of PSD-95 *versus* MAGI-2 is a key to understanding the differential effect of these two related proteins on $\beta_1$AR internalization.

While PSD-95 and MAGI-2 have distinct distributions in the mammalian brain, their distributions do overlap significantly and it is likely that there are many neuronal populations where the two proteins are co-expressed. What are the likely consequences of this for $\beta_1$AR function and localization? PSD-95 and MAGI-2 have been reported to have a direct physical interaction via PDZ domain dimerization (39), and they also both bind with high affinity to the GKAP/SAPAP class of scaffolding proteins (55, 70, 71). Thus, in neurons expressing both PSD-95 and MAGI-2, it might be expected that the two proteins will bind both to each other and to various other synaptic components to help form the complex architecture of the post-synaptic density (72). Since both PSD-95 and MAGI-2 bind the $\beta_1$AR, they may work in a coordinated fashion to localize the $\beta_1$AR to synapses and regulate $\beta_1$AR function.

Our mutagenesis studies indicate that three of the last four residues of the $\beta_1$AR-CT are the key determinants of the interaction with MAGI-2 PDZ1. Interestingly, several other proteins known to bind PDZ1 of MAGI proteins have carboxyl-terminal motifs very similar to that of the $\beta_1$AR (SESKV). For example, neuroligin-1 is known to associate with MAGI-2 PDZ1 (55) and terminates in STTRV, meaning that it shares with the $\beta_1$AR the terminal valine residue, a basic residue at the $-1$ position, a hydroxyl-bearing amino acid (S/T) at the $-2$ position and a serine at the $-4$ position. Another MAGI-2 binding partner is nRapGEP (57), which terminates in QVSAV and thus shares with the $\beta_1$AR the two residues determined by our mutagenesis studies to be the most important for MAGI-2 binding (the carboxyl-terminal S*X*V). The carboxyl terminus of a third MAGI-2-binding protein, mNET1 (64), is even more similar to the $\beta_1$AR-CT, terminating in KETLV. This motif conserves the three most important residues of the $\beta_1$AR-CT, at positions 0, $-2$, and $-3$. Peptide library screening experiments to determine the optimal motif for association with MAGI-2 PDZ1 have not yet been reported, but the ideal motif for binding to MAGI-2 PDZ1 may be approximated as E(S/T)*X*V, based on our work and the previous work cited here. Furthermore, the high affinity of the MAGI-2 PDZ1/$\beta_1$AR-CT interaction ($K_D$ = 10 nM) suggests that the $\beta_1$AR-CT contains a motif that is close to ideal for association with the PDZ1 domain of MAGI-2.

In both our co-immunoprecipitation studies and our immunofluorescence experiments, the association of $\beta_1$AR and MAGI-2 occurred constitutively but was further promoted by agonist stimulation of the receptor. Heptahelical receptors are known to undergo significant conformational changes following activation by agonist, and proteins that interact primarily with the third intracellular loop of heptahelical receptors, such as G proteins (73) and arrestins (74), usually associate preferentially with agonist-activated receptors. For proteins that interact with the carboxyl termini of heptahelical receptors, the literature is more equivocal. In some cases, interactions are promoted by agonist, as in the cases of NHERF association with the $\beta_2$-adrenergic receptor (33) and cortactin-binding protein 1 association with the SSTR2 somatostatin receptor (75). In other cases, such as the interaction of PSD-95 with the $\beta_1$AR (24), no evidence for agonist-dependent regulation is evident. The reason why the association of the $\beta_1$AR with MAGI-2 but not PSD-95 should be promoted by agonist is not clear, but it may have to do with the aforementioned differential lipid modification of the two proteins. PSD-95 is known to be membrane-anchored through palmitoylation (69) while MAGI-2 is not, and thus MAGI-2 may be more prone than PSD-95 to rapid translocation within the cell in response to transient stimulation such as agonist activation of a receptor. Alternatively, since PSD-95 and MAGI-2 differ in the arrangement of their domains, they may also differ with regard to the accessibility of their PDZ domains for binding to the $\beta_1$AR. The two proteins clearly bind to the same motif at the distal $\beta_1$AR carboxyl terminus, but it may be that PSD-95 association is insensitive to global changes in receptor conformation while the larger MAGI-2 requires the $\beta_1$AR to undergo an agonist-induced conformational change in order to have full access to the carboxyl terminus of the receptor.

The $\beta_1$- and $\beta_2$-adrenergic receptors share 54% sequence identity, bind to the same endogenous ligands, and couple predominantly to the same G protein ($G_s$), yet in many cells they are known to exert markedly different physiological effects (76–78). Since $\beta$-adrenergic receptors are the molecular targets for a number of commonly prescribed therapeutics, the mechanisms by which the various $\beta$AR subtypes can have differential effects on cellular processes have been an area of intense research interest. We offer the perspective that the cellular actions of $\beta$-adrenergic receptors are largely determined by the set of cytoplasmic proteins with which they can associate. Interactions that are common to all $\beta$AR subtypes, such as $G_s$ (73) and arrestins (74), probably underlie cellular actions that are common to all the subtypes. Conversely, interactions that occur differentially between $\beta$AR subtypes may be expected to underlie cellular actions that are distinct between $\beta$AR subtypes. Previously reported examples of unique interactions between cytoplasmic proteins and specific $\beta$-adrenergic receptor subtypes include the interaction of the NHERF proteins with the $\beta_2$AR (33, 34, 56), the interaction of the endophilins with the $\beta_1$AR (67), the interaction of Src with the $\beta_3$AR (47), and the interaction of PSD-95 with the $\beta_1$AR (24). The interaction of the $\beta_1$AR with MAGI-2, as reported here, adds to the short list of proteins known to bind specifically to one subtype of $\beta$-adrenergic receptor. Elucidation of the molecular basis for the unique cellular actions of the various $\beta$-adrenergic receptors may contribute to the development of novel therapeutics that can selectively target the signaling pathways of the individual receptor subtypes.

*Acknowledgments*—We thank Robert Lefkowitz for support and advice in the early stages of this project, Jeremy Blitzer for contributions to preliminary aspects of these studies, Amanda Castleberry for excellent technical assistance, and Junqi He and Liaoyuan Hu for helpful discussions. We also thank Morgan Sheng for providing PSD-95 cDNA, Thomas Michel for providing nNOS cDNA, Shirish Shenolikar and Ed Weinman for providing NHERF-1 cDNA, Kenneth Minneman for providing $\alpha_{1A}$AR cDNA, and Hitoshi Kurose for providing the HA-$\beta_1$AR expression construct.

REFERENCES

1. Hopkins, W. F., and Johnston, D. (1988) *J. Neurophysiol.* **59,** 667–687
2. Huang, Y. Y., and Kandel, E. R. (1996) *Neuron* **16,** 611–617
3. Thomas, M. J., Moody, T. D., Makhinson, M., and O'Dell, T. J. (1996) *Neuron* **17,** 475–482
4. Watanabe, Y., Ikegaya, Y., Saito, H., and Abe, K. (1996) *Neuroscience* **71,** 1031–1035
5. Bramham, C. R., Bacher-Svendsen, K., and Sarvey, J. M. (1997) *Neuroreport* **8,** 719–724
6. Katsuki, H., Izumi, Y., and Zorumski, C. F. (1997) *J. Neurophysiol.* **77,** 3013–3020

7. Ikegaya, Y., Nakanishi, K., Saito, H., and Abe, K. (1997) *Neuroreport* **8,** 3143–3146
8. Moody, T. D., Thomas, M. J., Makhinson, M., and O'Dell, T. J. (1998) *Brain Res.* **794,** 75–79
9. Winder, D. G., Martin, K. C., Muzzio, I. A., Rohrer, D., Chruscinski, A., Kobilka, B., and Kandel, E. R. (1999) *Neuron* **24,** 715–726
10. Cohen, A. S., Coussens, C. M., Raymond, C. R., and Abraham, W. C. (1999) *J. Neurophysiol.* **82,** 3139–3148
11. Wang, S. J., Cheng, L. L., and Gean, P. W. (1999) *J. Neurosci.* **19,** 570–577
12. Flexner, J. B., Flexner, L. B., Church, A. C., Rainbow, T. C., and Brunswick, D. J. (1985) *Proc. Natl. Acad. Sci. U. S. A.* **82,** 7458–7461
13. Cahill, L., Prins, B., Weber, M., and McGaugh, J. L. (1994) *Nature* **371,** 702–704
14. Nielson, K. A., and Jensen, R. A. (1994) *Behav. Neural Biol.* **62,** 190–200
15. van Stegeren, A. H., Everaerd, W., Cahill, L., McGaugh, J. L., and Gooren, L. J. (1998) *Psychopharmacology* (*Berl.*) **138,** 305–310
16. Przybyslawski, J., Roullet, P., and Sara, S. J. (1999) *J. Neurosci.* **19,** 6623–6628
17. McGaugh, J. L. (2000) *Science* **287,** 248–251
18. Cash, R., Raisman, R., Lanfumey, L., Ploska, A., and Agid, Y. (1986) *Brain Res.* **370,** 127–135
19. Waeber, C., Rigo, M., Chinaglia, G., Probst, A., and Palacios, J. (1991) *Synapse* **8,** 270–280
20. Mantyh, P. W., Rogers, S. D., Allen, C. J., Catton, M. D., Ghilardi, J. R., Levin, L. A., Maggio, J. E., and Vigna, S. R. (1995) *J. Neurosci.* **15,** 152–164
21. Strader, C. D., Pickel, V. M., Joh, T. H., Strohsacker, M. W., Shorr, R. G., Lefkowitz, R. J., and Caron, M. G. (1983) *Proc. Natl. Acad. Sci. U. S. A.* **80,** 1840–1844
22. Aoki, C., Joh, T. H., and Pickel, V. M. (1987) *Brain Res.* **437,** 264–282
23. Garner, C. C., Nash, J., and Huganir, R. L. (2000) *Trends Cell Biol.* **10,** 274–280
24. Hu, L. A., Tang, Y., Miller, W. E., Cong, M., Lau, A. G., Lefkowitz, R. J., and Hall, R. A. (2000) *J. Biol. Chem.* **275,** 38659–38666
25. Sheng, M., and Sala, C. (2001) *Annu. Rev. Neurosci.* **24,** 1–29
26. Frielle, T., Collins, S., Daniel, K. W., Caron, M. G., Lefkowitz, R. J., and Kobilka, B. K. (1987) *Proc. Natl. Acad. Sci. U. S. A.* **84,** 7920–7924
27. Nicholas, A. P., Pieribone, V. A., and Hokfelt, T. (1993) *Neuroscience* **56,** 1023–1039
28. Nicholas, A. P., Hokfelt, T., and Pieribone, V. A. (1994) *Trends Pharmacol. Sci.* **17,** 245–255
29. Cho, K. O., Hunt, C. A., and Kennedy, M. B. (1992) *Neuron* **9,** 929–942
30. Brenman, J. E., Chao, D. S., Gee, S. H., McGee, A. W., Craven, S. E., Santillano, D. R., Wu, Z., Huang, F., Xia, H., Peters, M. F., Froehner, S. C., and Bredt, D. S. (1996) *Cell* **84,** 757–767
31. Fukaya, M., Ueda, H., Yamauchi, K., Inoue, Y., and Watanabe, M. (1999) *Neurosci. Res.* **33,** 111–118
32. Wood, J. D., Yuan, J., Margolis, R. L., Colomer, V., Duan, K., Kushi, J., Kaminsky, Z., Kleiderlein, J. J., Sharp, A. H., and Ross, C. A. (1998) *Mol. Cell Neurosci.* **11,** 149–160
33. Hall, R. A., Premont, R. T., Chow, C.-W., Blitzer, J. T., Pitcher, J. A., Claing, A., Stoffel, R. H., Barak, L. S., Shenolikar, S., Weinman, E. J., Grinstein, S., and Lefkowitz, R. J. (1998) *Nature* **392,** 626–630
34. Hall, R. A., Ostedgaard, L. S., Premont, R. T., Blitzer, J. T., Rahman, N., Welsh, M. J., and Lefkowitz, R. J. (1998) *Proc. Natl. Acad. Sci. U. S. A.* **95,** 8496–8501
35. Hall, R. A., and Soderling, T. R. (1997) *J. Biol. Chem.* **272,** 4135–4140
36. Wu, X., Hepner, K., Castelino-Prabhu, S., Do, D., Kaye, M. B., Yuan, X. J., Wood, J., Ross, C., Sawyers, C. L., and Whang, Y. E. (2000) *Proc. Natl. Acad. Sci. U. S. A.* **97,** 4233–4238
37. Ide, N., Hata, Y., Deguchi, M., Hirao, K., Yao, I., and Takai, Y. (1999) *Biochem. Biophys. Res. Commun.* **256,** 456–461
38. Kawajiri, A., Itoh, N., Fukata, M., Nakagawa, M., Yamaga, M., Iwamatsu, A., and Kaibuchi, K. (2000) *Biochem. Biophys. Res. Commun.* **273,** 712–717
39. Hirao, K., Hata, Y., Yao, I., Deguchi, M., Kawabe, H., Mizoguchi, A., and Takai, Y. (2000) *J. Biol. Chem.* **275,** 2966–2972
40. Salahpour, A., Angers, S., and Bouvier, M. (2000) *Trends Endocrinol. Metab.* **11,** 163–168
41. Hebert, T. E., Moffett, S., Morello, J. P., Loisel, T. P., Bichet, D. G., Barret, C., and Bouvier, M. (1996) *J. Biol. Chem.* **271,** 16384–16392
42. Hebert, T. E., Loisel, T. P., Adam, L., Ethier, N., Onge, S. S., and Bouvier, M. (1998) *Biochem. J.* **330,** 287–293
43. Angers, S., Salahpour, A., Joly, E., Hilairet, S., Chelsky, D., Dennis, M., and Bouvier, M. (2000) *Proc. Natl. Acad. Sci. U. S. A.* **97,** 3684–3689
44. Premont, R. T., and Hall, R. A. (2001) *Methods Enzymol.* **343,** 613–623
45. Kornau, H. C., Schenker, L. T., Kennedy, M. B., Seeburg, P. H. (1995) *Science* **269,** 1737–1740
46. Kim, E., Niethammer, M., Rothschild, A., Jan, Y. N., and Sheng, M. (1995) *Nature* **378,** 85–88
47. Cao, W., Luttrell, L. M., Medvedev, A. V., Pierce, K. L., Daniel, K. W., Dixon, T. M., Lefkowitz, R. J., and Collins, S. (1999) *J. Biol. Chem.* **275,** 38131–38134
48. Irie, M., Hata, Y., Takeuchi, M., Ichtchenko, K., Toyoda, A., Hirao, K., Takai, Y., Rosahl, T. W., and Sudhof, T. C. (1997) *Science* **277,** 1511–1515
49. Niethammer, M., Valtschanoff, J. G., Kapoor, T. M., Allison, D. W., Weinberg, T. M., Craig, A. M., and Sheng, M. (1998) *Neuron* **20,** 693–707
50. Zhang, W., Vazquez, L., Apperson, M., and Kennedy, M. B.(1999) *J. Neurosci.* **19,** 96–108
51. Furuyashiki, T., Fujisawa, K., Fujita, A., Madaule, P., Uchino, S., Mishina, M., Bito, H., and Narumiya, S. (1999) *J. Neurosci.* **19,** 109–118
52. Tezuka, T., Umemori, H., Akiyama, T., Nakanishi, S., and Yamamoto, T. (1999) *Proc. Natl. Acad. Sci. U. S. A.* **96,** 435–440
53. Firestein, B. L., Brenman, J. E., Aoki, C., Sanchez-Perez, A. M., El-Husseini, A. E., and Bredt, D. S. (1999) *Neuron* **24,** 659–672
54. Huang, Y. Z., Won, S., Ali, D. W., Wang, Q., Tanowitz, M., Du, Q. S., Pelkey, K. A., Yang, D. J., Xiong, W. C., Salter, M. W., and Mei, L. (2000) *Neuron* **26,** 443–455
55. Hirao, K., Hata, Y., Ide, N., Takeuchi, M., Irie, M., Yao, I., Deguchi, M., Toyoda, A., Sudhof, T. C., and Takai, Y. (1998) *J. Biol. Chem.* **273,** 21105–21110
56. Cao, T. T., Deacon, H. W., Reczek, D., Bretscher, A., and von Zastrow, M. (1999) *Nature* **401,** 286–290
57. Ohtsuka, T., Hata, Y., Ide, N., Yasuda, T., Inoue, E., Inoue, T., Mizoguchi, A., and Takai, Y. (2000) *Biochem. Biophys. Res. Commun.* **265,** 38–44
58. Dobrosotskaya, I., Guy, R. K., and James, G. L. (1997) *J. Biol. Chem.* **272,** 31589–31597
59. Wu, Y., Dowbenko, D., Spencer, S., Laura, R., Lee, J., Gu, Q., and Lasky, L. A. (2000) *J. Biol. Chem.* **275,** 21477–21485
60. Mino, A., Ohtsuka, T., Inoue, E., and Takai, Y. (2000) *Genes Cells* **5,** 1009–1016
61. Dobrosotskaya, I. Y., and James, G. L. (2000) *Biochem. Biophys. Res. Commun.* **270,** 903–909
62. Shiratsuchi, T., Futamura, M., Oda, K., Nishimori, H., Nakamura, Y., and Tokino, T. (1998) *Biochem. Biophys. Res. Commun.* **247,** 597–604
63. Patrie, K. M., Drescher, A. J., Goyal, M., Wiggins, R. C., and Margolis, B. (2000) *J. Am. Soc. Nephrol.* **12,** 667–677
64. Dobrosotskaya, I. Y. (2001) *Biochem. Biophys. Res. Commun.* **283,** 969–975
65. Suzuki, T., Nguyen, C. T., Nantel, F., Bonin, H., Valiquette, M., Frielle, T., and Bouvier, M. (1992) *Mol. Pharmacol.* **41,** 542–548
66. Green, S. A., and Liggett, S. B. (1994) *J. Biol. Chem.* **269,** 26215–26219
67. Tang, Y., Hu, L. A., Miller, W. E., Ringstad, N., Hall, R. A., Pitcher, J. A., DeCamilli, P., and Lefkowitz, R. J. (1999) *Proc. Natl. Acad. Sci. U. S. A.* **96,** 12559–12564
68. Shiina, T., Kawasaki, A., Nagao, T., and Kurose, H. (2000) *J. Biol. Chem.* **275,** 29082–29090
69. Topinka, J. R., and Bredt, D. S. (1998) *Neuron* **20,** 125–134
70. Kim, E., Naisbitt, S., Hsueh, Y. P., Rao, A., Rothschild, A., Craig, A. M., and Sheng, M. (1997) *J. Cell Biol.* **136,** 669–678
71. Takeuchi, M., Hata, Y., Hirao, K., Toyoda, A., Irie, M., and Takai, Y. (1997) *J. Biol. Chem.* **272,** 11943–11951
72. Sheng, M. (2001) *Proc. Natl. Acad. Sci. U. S. A.* **98,** 7058–7061
73. Dohlman, H. G., Thorner, J., Caron, M. G., and Lefkowitz, R. J. (1991) *Annu. Rev. Biochem.* **60,** 653–688
74. Krupnick, J. G., and Benovic, J. L. (1998) *Annu. Rev. Pharmacol. Toxicol.* **38,** 289–319
75. Zitzer, H., Richter, D., and Kreienkamp, H. J. (1999) *J. Biol. Chem.* **274,** 18153–18156
76. Xiao, R. P., Cheng, H., Zhou, Y. Y., Kuschel, M., and Lakatta, E. G. (1999) *Circ. Res.* **85,** 1092–1100
77. Steinberg, S. F. (1999) *Circ. Res.* **85,** 1101–1111
78. Steinberg, S. F. (2000) *Circ. Res.* **87,** 1079–1082